Carbon 227 (2024) 119262

Contents lists available at ScienceDirect

Carbon

journal homepage: www.elsevier.com/locate/carbon

Catalytic synergy: N,P modification of activated carbon for improved 1-chloro-4-nitrobenzene reduction

Edgar S. Duran-Uribe, Antonio Sepúlveda-Escribano, Enrique V. Ramos-Fernandez *

Universidad de Alicante, Departamento de Química Inorgánica – Instituto Universitario de Materiales de Alicante (IUMA), Apartado 99, Alicante, 03080, Spain

ARTICLE INFO

Keywords:
N and P codoped carbon
Nitroarene hydrogenation
Metal-free catalyst

ABSTRACT

Carbon materials have emerged as a new generation of catalysts for the crucial industrial hydrogenation of nitroarenes. Activated carbon, known for its cost-effectiveness and facile modifiability, stands out among various carbon materials. This study focuses on the preparation of N and P co-doped carbons for catalysing the hydrogenation of 1-chloro-4-nitrobenzene. Comprehensive characterisation using thermal analysis (TGA-MS), X-ray photoelectron spectroscopy (XPS), Raman spectroscopy, N_2 adsorption at −196 °C, and ICP-MS was performed. The synergistic effect of N and P was evident, with co-doped carbons outperforming their mono-doped counterparts, underscoring the significance of nitrogen. N,P-codoped activated carbon emerges as a promising, active, stable, and selective metal-free catalyst for the hydrogenation of 1-chloro-4-nitrobenzene, leading to 4-chloroaniline.

1. Introduction

Aromatic amines constitute crucial building blocks in the chemical industry for the preparation of high-value compounds such as fertilisers, medicines, and fuels [1]. For example, *p*-chloroaniline, a vital aromatic amine, is critical in producing dyes, pigments, and chemicals for agricultural applications [2]. The synthesis of substituted anilines encompasses various methods, with the reduction of nitroarenes emerging as one of the most technologically feasible and atomically efficient approaches [1–3]. Catalytic reduction of nitroarenes is a particularly noteworthy route in this context [1]. Various catalysts have been investigated for this reaction, including those derived from noble and non-noble metals [3]. Catalysts based on noble metals exhibit exceptional catalytic activity but often suffer from selectivity issues toward the desired substituted aniline [3]. Conversely, non-noble metal catalysts, such as those utilising cobalt (Co), have demonstrated high activity and selectivity [4]. Nevertheless, concerns related to potential leaching, fluctuating metal prices, and environmental impact have prompted a new approach to these catalysts' design [3,5]. Consequently, considerable efforts have been directed toward developing metal-free catalysts that are both environmentally friendly and economically viable.

Carbon-based catalysts have appeared as the next-generation catalysts for hydrogenating nitroarenes [5] due to their chemical stability, tunable physicochemical properties, and diverse fabrication methods [3,5]. However, studies of carbon materials for the hydrogenation of nitroarenes have focused more on their use as catalyst support than as a catalyst by itself [5,6]. In the realm of metal-free carbon catalysts, the attention has been given to different carbonaceous materials such as carbon nanotubes (CNTs), graphene and activated carbon [5]. This nano-carbon-based catalyst utilisation can be attributed to their substantial surface area and facile surface chemistry modification [7]. Especially surface chemistry plays a pivotal role in the design of metal-free catalysts for hydrogenation [5,7]. Nevertheless, while nanotubes enjoy popularity, there is a need for more comprehensive studies on activated carbons in the context of the reaction mentioned above. Activated carbons offer the same interesting properties as CNTs, such as easy modification of their surface chemistry and high specific surface area, all with greater cost-effectiveness, which is always an interesting issue in academic and industrial catalysis [7].

As mentioned earlier, surface chemistry is of great catalytic importance and can be easily modified by the inclusion of heteroatoms [8]. Heteroatoms are species such as oxygen (O), boron (B), sulfur (S), halogens, nitrogen (N), or phosphorus (P), which can interact with the carbonaceous structure, primarily altering the charge distribution in the carbon [7,8]. Moreover, the nature of the heteroatom introduces various structural modifications and influences the creation of acidic and basic sites, directly impacting species adsorption and catalytic activity [9]. Consequently, the properties of carbon can be tailored to meet the

* Corresponding author.
E-mail address: enrique.ramos@ua.es (E.V. Ramos-Fernandez).

https://doi.org/10.1016/j.carbon.2024.119262
Received 5 March 2024; Received in revised form 17 May 2024; Accepted 18 May 2024
Available online 21 May 2024

specific demands of the reaction.

N-doping has significant attention and progress among researchers due to its ease of incorporation into the carbonaceous lattice since N (0.65 Å) and C (0.70 Å) have similar atomic radii [7,10,11], resulting in the nitrogen groups shown in Scheme 1. Furthermore, nitrogen's higher electronegativity (3.04) compared to carbon (2.55) results in the formation of basic sites, which can affect the activity in hydrogenation reactions. Hence, numerous investigations have been conducted employing diverse N-doped carbocatalysts for the hydrogenation of nitroarenes [1,5,7,10–12]. For example, in a recent study, Shan et al. synthesised N-doped CNTs using melamine as a precursor, achieving commendable activities across various substrates [13]. They found some results suggesting the quaternary-N species as one of the most active species in the reaction [13]. However, the role of nitrogen groups in the hydrogenation of nitroarenes is still a matter of discussion in the field.

In contrast, phosphorus, another heteroatom with versatile applications, has received comparatively less attention than nitrogen. Phosphorus, with a larger atomic radius than carbon (0.98 Å), poses challenges for structural integration, leading to a more significant generation of defects [14]. However, its lower electronegativity (2.19) compared to carbon promotes the formation of acid sites, showcasing its potential for catalytic applications [14,15]. Scheme 1 illustrates the most prevalent N and P groups. Some works using CNTs and phosphorus-doped activated carbons showed high activities towards the corresponding aniline and a dependence of the activity on the number of defects and the P content [16,17]. Therefore, both N- and P-doped carbocatalysts have shown promising results for use in the reaction mentioned above.

The incorporation of heteroatoms into carbonaceous materials can be achieved through various methods, including the pyrolysis of precursors containing the heteroatom, such as polymers [8]. Alternatively, carbon modification with doping agents is a widely adopted approach due to its simplicity [8,14]. Several doping agents are employed to produce N-doped carbons, with ammonia, urea, and melamine being commonly used, particularly for their cost-effectiveness and low toxicity [10]. In the case of P-doped carbons, prevalent dopants include phosphoric acid and sodium hypophosphite [14]. Notably, phytic acid stands out as a promising yet less explored precursor attributed to its biomass source, offering potential economic and sustainable advantages [14,16].

An interesting approach in the development of doped carbon catalysts is co-doping, which involves the introduction of two different types of atoms into the carbonaceous network [5]. This methodology has demonstrated promising outcomes, revealing cooperative effects between distinct species, as observed in N–S and N–O [5,18]. However, these co-doped systems on carbons are predominantly used as catalyst supports for metals. Some studies with the N–P system have shown good stability and activity; however, they have focused on its use as a catalyst for photo thermochemical reactions or employing expensive carbocatalysts such as graphene [9,19]. Consequently, investigations into co-doped N, P systems on activated carbons for their utility as metal-free catalysts in the hydrogenation of nitroarenes remain relatively limited. Hence, recognising the potential of the N, P system for nitroarene reduction, this study proposes the utilisation of activated carbon-based catalysts in a co-doped configuration. Our investigation demonstrates enhanced catalytic activity when introducing N and P simultaneously into the system. Notably, P-doping on an N-doped carbon revealed a superior stabilisation of P groups compared to an undoped carbon. Moreover, these catalysts exhibited robust activities, high selectivities, and considerable stability. Remarkably, upon multiple recycling cycles, an enhancement in catalytic activity was observed, attributed to surface modification.

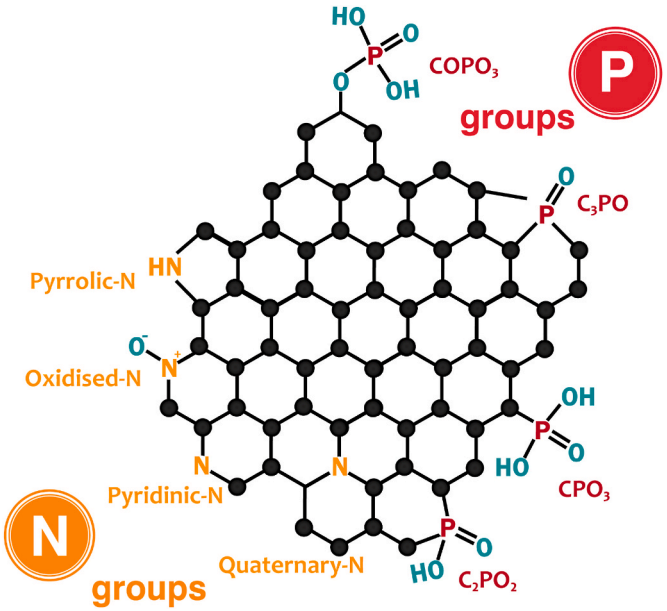

Scheme 1. Common N- and P- containing groups in carbon materials.

2. Experimental section

2.1. Materials synthesis

A commercial low-ash activated carbon, RGC-30, obtained from West-Vaco Co, was modified to synthesise doped carbons. The first step involved nitrogen doping using melamine as a precursor, based on the methodology proposed by Villora-Picó et al. [4]. A mixture of RGC-30 and melamine (99 %, Sigma Aldrich) in a 1:4 wt ratio was mechanically homogenised and pyrolysed in a tube furnace under an inert N_2 atmosphere (100 ml min^{-1}). The heating ramp was set at 3 °C·min^{-1}, and an 800 °C isotherm was maintained for 1 h. The resulting material from this pyrolysis process was denoted as RMel_800.

Subsequently, phosphorus doping was conducted on the RMel_800 sample using phytic acid (PA) as a precursor (50 wt% in water, Sigma Aldrich). Homogeneous mixtures of RMel_800 carbon with phytic acid were prepared, varying the mass ratio of PA to RMel_800 to 1.5, 2.0, and 5.0. The mixtures were dried in an oven at 180 °C for 16 h. The materials underwent pyrolysis in a tube furnace under an inert nitrogen atmosphere (100 ml min^{-1}), employing a heating ramp of 3 °C·min^{-1} and a 900 °C isotherm period for 1 h. The resulting materials were labelled as MelPhyx_900P, where "x" represents the mass ratio of PA used, "900" identifies the pyrolysis temperature, and "P" indicates the pre-polymerization treatment of the PA. For example, MelPhy1.5_900P indicates a co-doped carbon from a mixture of RMel_800:PA of 1:1.5 pyrolysed at 900 °C with a pre-polymerization process of phytic acid, whereas MelPhy1.5_900 indicates the same initial mixture mentioned above, but without the pre-polymerizations treatment.

On the other hand, P-doped carbons were synthesised. For this, a similar synthesis to the MelPhy series was performed, using RGC-30 as the base carbon. The materials were denoted as RPhy*x*_*y*P, where "*x*" is the mass ratio between RGC: PA, "*y*" is the pyrolysis temperature, and "P" refers to the pre-polymerization of the phytic acid on the carbon. For example, RPhy1.5_800P indicates a sample synthesised from a mixture of 1:1.5 of RGC-30:PA, pyrolysed at 800 °C with a pre-polymerization treatment.

2.2. Materials characterization

To determine the thermal characteristics of the precursors, thermogravimetric analysis (TGA) was performed using a TGA/STA 449 F5 Jupiter from NETZSCH. The TGA measurements were executed over a temperature range from room temperature to 1000 °C, employing a heating ramp of 10 °C·min^{-1} under an inert atmosphere. N_2 adsorption isotherms were obtained at −196 °C, utilising a Quantachrome

Instrument AUTOSORB-iQ-XR-2. Prior to the adsorption measurements, samples were degassed at 250 °C for 4 h under vacuum using a Quantachrome Instrument Autosorb Degasser. Raman spectroscopy measurements were carried out on a Jasco NRS-5100 Raman machine employing a 633 nm laser and 600 lines per mm slit. X-ray photoelectron spectroscopy (XPS) was conducted with a K-Alpha spectrometer (Thermo Scientific). All spectra were collected using Mg-Kα radiation monochromatised by a double crystal monochromator with a hemispherical analyser. The binding energy for the XPS measurements was calibrated using the 1s transition of C in the C=C bond (284.60 eV). Thermogravimetric analysis-mass spectrometry (TGA-MS) was performed using a TGA/STA 449 F5 Jupiter coupled to a mass spectrometer Aeolos QMS 403 Quadro, both from NETZSCH. Mass spectrometric measurements with an inductive coupling plate (ICP-MS 8900, Agilent) were carried out to determine the total P content in the carbons. For this purpose, microwave digestion (Milestone Ultrawave) in aqua regia of the materials to be studied was previously done.

2.3. Catalytic test

Following the doping treatment, the catalysts underwent testing for the hydrogenation of 1-chloro-4-nitrobenzene (1-C-4NB). The catalytic experiments were conducted under atmospheric pressure in a 100 mL three-neck round-bottom flask equipped with an aliquot system. The experimental conditions included 50 mL of a 50 mM solution of 1C–4NB in ethanol, 100 mg of catalyst, and 22 mmol of hydrazine hydrate (35 wt % in H_2O), which served as the reducing agent. The catalytic system was maintained at 80 °C and 300 rpm. The samples were analysed using a gas chromatograph with a mass spectrometer and an HP-5 capillary column, employing helium as the carrier gas. The recycling test replicated the conditions above. To this end, the catalyst was recovered post-reaction through filtration and ethanol washing, followed by overnight drying in an oven at 60 °C.

3. Results

N,P-codoped catalysts (MelPhy-series) were synthesised by pyrolysis of RGC-30 with precursors of the corresponding heteroatoms, melamine as the N source and phytic acid as the P source. This doping treatment was performed in two steps. The first consisted of preparing nitrogen-doped carbon using RGC-30 and melamine. Subsequently, the N-doped carbon was used as a base carbon for P-doping using PA. A preliminary study on the thermal behaviour of the precursors using thermogravimetric analysis (TGA) was performed. To this end, a mechanical mixture of RGC-30 with melamine in a 1:4 wt ratio of carbon to dopant was studied (RMel_Raw). The mixture of RMel_Raw shows mainly two mass loss processes (Fig. 1 - green line). These two steps occur between 230 and 650 °C and relate to melamine's thermal dehydration and condensation to form carbon nitride and release NH_3 [20,21]. Subsequently, at temperatures higher than 650 °C, there is a gradual but slower mass loss, which may be attributed to the sublimation of the carbon nitride in the form of N_2 and HCN, which will react with the raw carbon [22]. Therefore, to obtain a carbon without melamine decomposition residues, the pyrolysis temperature was chosen to be higher than 650 °C. In this case, we chose 800 °C, and the sample was named RMel_800.

On the other hand, the thermogram related to the RMel_800 treated with phytic acid at 180 °C (MelPhy_Raw-blue line, Fig. 1) has different behaviour from the RMel_Raw mixture, showing similar thermal degradation as the RGC-30 treated with phytic acid at 180 °C (RPhy_Raw, purple line, Fig. 1). Five stages of mass loss were identified during the analysis. The initial stage, spanning temperatures between 60 °C and 108 °C, is associated with the removal of residual water present in the precursors. Following this, two distinct stages occur in the range of 108 °C–450 °C, marked by the dehydration of phytic acid via the condensation and decomposition of the hydroxyl (OH) groups [23].

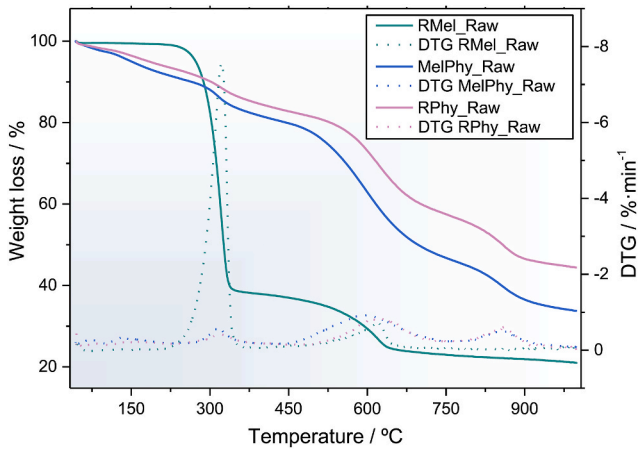

Fig. 1. TGA (solid line) and DTG (dots line) from the RGC-30 with melamine mixture, RMel_Raw (green), RMel_800 with a pre-polymerization of phytic acid at 180 °C, MelPhy_Raw (blue), and RGC-30 with a pre-polymerization of phytic acid at 180 °C, RPhy_Raw (purple). (A colour version of this figure can be viewed online.)

Subsequently, a substantial mass loss becomes evident, spanning the temperature interval from 450 °C to 760 °C, predominantly attributed to the decomposition of phytates [23]. Finally, a fifth stage emerges, representing the complete carbonisation of phytic acid on RGC-30, occurring at temperatures exceeding 760 °C. Consequently, from TGA data, 900 °C was selected as the pyrolysis temperature for the mix of RMel_Raw and PA to ensure the thermal decomposition of the PA; furthermore, different RMel_Raw: PA ratios were used (1.5, 2.0, 5.0) to study the effect of the amount of PA in the final carbon.

The raw carbon sample (RGC-30) exhibits a combination of type I and type IV isotherms, indicative of a micro-mesoporous carbon structure [24] (Fig. 2). Furthermore, an H4-hysteresis loop corroborates the presence of mesoporos. The N_2 adsorption data, as summarised in Table 1, reveal that RGC-30 possesses a substantial surface area over 1518 $m^2\ g^{-1}$. Additionally, it boasts a total pore volume (V_{total}) of 1.14 $cc{\cdot}g^{-1}$, consisting of a total micropore volume (V_{micro}) of 0.52 $cc{\cdot}g^{-1}$ and a mesopore volume (V_{meso}) of 0.62 $cc{\cdot}g^{-1}$. These characteristics show that RGC-30 is a material with highly developed porosity, with potential use in catalytic applications to avoid diffusional issues and ensure the kinetic regime during the hydrogenation reaction. When treating RGC-30 with melamine at 800 °C (RMel_800), a typical isotherm of a

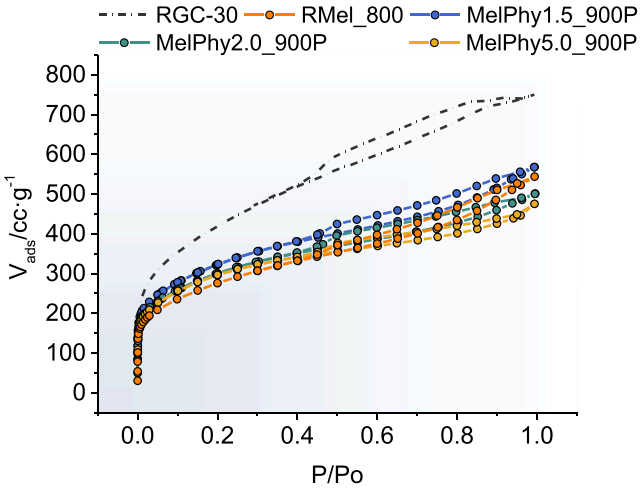

Fig. 2. Nitrogen adsorption isotherms adsorption at −196 °C for de N,P- doped carbons. (A colour version of this figure can be viewed online.)

Table 1
Textural parameters from nitrogen adsorption isotherms for the N,P-doped carbons.

Catalyst	S_{BET} ($m^2 \cdot g^{-1}$)	V_{Total} ($cc \cdot g^{-1}$)	V_{micro} ($cc \cdot g^{-1}$)	V_{meso} ($cc \cdot g^{-1}$)
RGC-30	1518	1.14	0.52	0.62
RMel_800	992	0.81	0.33	0.58
MelPhy1.5_900P	1158	0.83	0.39	0.44
MelPhy2.0_900P	1028	0.75	0.36	0.39
MelPhy5.0_900P	1002	0.68	0.36	0.32

micro-mesoporous material is still observed, accompanied by a change in the textural parameters of the final carbon (Fig. 2, Table 1). A significant reduction in the adsorption capacity at low relative pressure was evident, indicating the primary impact of melamine treatment on microporosity. This may be related to the NH_3 released during the thermal decomposition of melamine, which has been shown to alter the textural properties of coals at high temperatures [25]. Conversely, marginal alterations were noted in relation to the V_{meso} compared to the RGC-30. Due to these changes in textural parameters, a substantial modification in specific surface area is appreciated.

Like the other investigated carbons, the MelPhy samples displayed a characteristic micro-mesoporous material adsorption isotherm, similar to its starting material (RMel) (Fig. 2). A modest improvement in the specific surface area can be observed, which is associated with a slight increase in the V_{micro} (Table 1). Additionally, an increase in the amount of PA used for doping decreases textural parameters, particularly in mesoporosity. Despite these subtle changes, they do not significantly impact adsorption capacity. Consequently, all samples can be regarded as having a similar porous texture.

Raman measurements were carried out to observe how the doping treatments affect the structure of the carbons (Fig. 3a–e). The spectra show two prominent bands at 1350 cm^{-1} or 1590 cm^{-1}, related to carbon materials' D and G bands [26–28]. After normalisation, the signals were deconvoluted using the Gaussian function. The deconvoluted spectra of the investigated materials in the range of 750 cm^{-1} to 2000 cm^{-1} are composed of 4 contributions. The first peak at ~1200 cm^{-1}, D4, is related to the A_{1g} mode of disordered graphite and ionic impurity [27,29]. Later an intense peak at ~1345 cm^{-1} is observed, associated to the D1 band, which is related to high density of phonon states near the Brillouin zone corner, from disordered graphite lattice (A_{1g}) [27,29]. The D3 is observed at ~1500 cm-1 at higher Raman frequency, related to amorphous carbon [27,29]. Finally, at ~1595 cm^{-1}, the fourth contribution corresponds to the G band; this peak is related to the E_{2g} symmetry of a graphitic structure (ordered carbon) [26–29]. Therefore, the structure of these materials is composed of partially ordered amorphous carbon.

To determine the degree of graphitisation of the carbons, the I_{D1}/I_G and R2 index were calculated (Fig. 3f). The I_{D1}/I_G ratio indicates the density of defects present in these materials; as it increases, the disordered, amorphous and/or defective portion of the carbon increases [26,27,29]. After treatment with melamine at 800 °C (RMel_800), there is an increase in the I_{D1}/I_G index, which is related to an increase in the density of defects in the carbon [26,27,29]. On the other hand, when the sample RMel_800 is treated with phytic acid at 900 °C, the defect density tends to decrease (I_{D1}/I_G value decreases). This may be because the structure tends to become more organised when the carbon is thermally treated at a high temperature [30]. However, the ratio of intensities between the D1 and G bands has a certain degree of statistical uncertainty. Consequently, Beyssac et al. proposed the R2 parameter as a statistically more accurate and less variable way to measure the degree of ordering of carbon [29]. This calculation is somewhat similar to the I_{D1}/I_G; however, instead of using the intensity ratio, the areas of the peaks D1, D2 and G are used, according to **equation (1)** [27,29]. Thus, if R2>0.5, the coal has a high defect density, whereas if R2<0.5, the carbon can be considered to have a highly ordered structure [29]. As shown in Fig. 3f, the R2 values are greater than 0.5. Therefore, although there is a slight tendency for the structure to become more ordered after treatment with

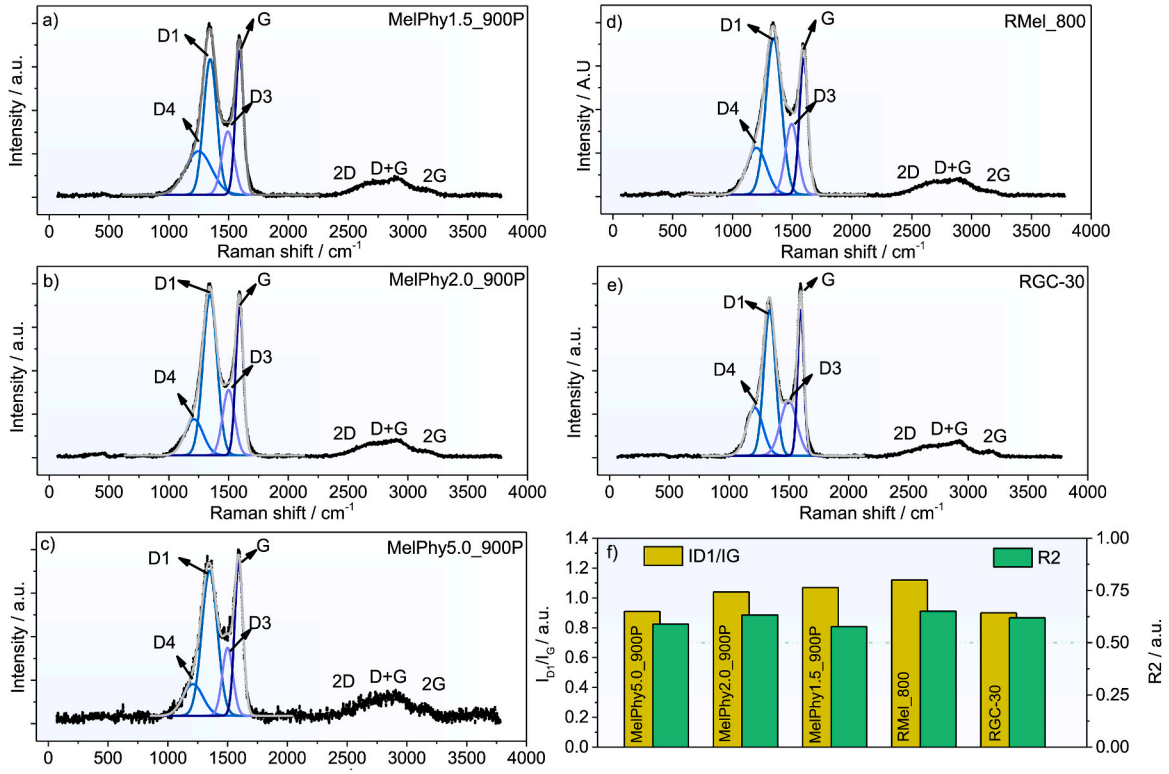

Fig. 3. Raman spectra of the investigated carbons: a) MelPhy1.5_900, b) Melphy2.0_900P, c) MelPhy5.0_900P, d) RMel_800 and e) RGC-30 carbons, f) I_{D1}/I_G and R2 index from Raman data. (A colour version of this figure can be viewed online.)

phytic acid at 900 °C, this ordering is not significant, and the resulting material is a poorly ordered carbon

$$\boldsymbol{R2} = D1/(G + D1 + D2) \quad \text{Equation 1}$$

Finally, at higher Raman frequencies (around 2000-3500 cm-1), weak signals related to the D- and G-band overtones are observed: 2D, D + G and 2G.

ICP-MS measurements determined the P content introduced into the catalysts (Table 2). In these measurements, there is a slight increase in the P content in the catalyst as the mass of PA initially used increases in relation to RMel_800. The P content varies from 5.3 wt% for an initial mass ratio (PA: RMel_800) of 1.5:1 to 6.9 wt% for the highest ratio (PA: RMel_800 of 5:1 in the MelPhy5.0_900P sample).

Since oxygen surface groups on carbonaceous materials can decompose at different temperatures in the form of CO (28 m/z) and CO_2 (44 m/z) when treated in an inert atmosphere [31], thermogravimetry coupled to mass spectrometry (TGA-MS) measurements were performed (Fig. 4). The TGA-MS data for the RGC-30 carbon shows the presence of certain oxygenated groups, which decompose at high temperatures (T > 600 °C), such as lactones (LC, decomposition temperature: 600–800 °C in CO_2) and carbonyl/quinone (Cnyl/QN, decomposition temperature: 700–950 °C in CO) [31]. In addition, a small contribstion of carboxylic acid (CA, decomposition temperature: 150-350 °C in CO_2) groups is observed [31].

Fig. 4a shows that the mass loss profile of the RMel_800 sample is similar to that of the RGC-30 sample up to 700 °C. Monitoring the TGA-released gases, a small peak in H_2O (18 m/z) over 100 °C was found (Fig. 4a), associated with desorption of ambient humidity, indicating a higher hydrophilicity compared to RGC-30. In addition, small changes in the CO and CO_2 signals (Fig. 4c) are observed compared to the RGC-30 signals. Firstly, the contribution in the CO_2 signal related to the CA remains unchanged. However, an increase of O-groups in the surface, such as Cnyl/QN and LC, and during melamine treatment was found. Lastly, an increase in both signals (CO and CO_2) related to the decomposition of pyrones (Py, decomposition temperature >900 °C) is observed [31]. However, the most interesting aspect of the TGA-MS of the RMel_800 sample is the signal of HCN (27 m/z) , where a peak above 800 °C can be observed, which is related to the decomposition of N-groups. This means that nitrogen was effectively incorporated into RGC-30 during melamine treatment. MelPhy samples have a different behaviour compared to RMel_800 and RGC-30. Firstly, a loss of mass is observed at low temperatures. In addition, a progressive mass loss rate is observed at higher temperatures (T > 800 °C). The initial mass loss is related to H_2O release (Fig. 4b), where a peak at 110 °C was observed in 18 m/z. This peak is associated with the desorption of ambient humidity due to the increase of the hydrophilicity after the treatment with PA. The amount of H_2O desorbed increases with the amount of PA used in the treatment and, consequently, with the P content measured from ICP-MS (Table 2). As outlined above, two mass fractions are followed, CO (28 m/z) and CO_2 (44 m/z), as they can provide information on the oxygenated and phosphorus functionalities of carbon [31,32]. Thus, in the CO and CO_2 signals of MelPhy samples, a peak is observed above 900 °C, which is an indication of the decomposition of P groups [32]. This peak can be associated with C–P=O_3, which gives rise to C–P species generating CO_2 and CO [14,32]. Furthermore, there is no evidence of the presence of C–O–P groups since no water generation or peaks above 700 °C in CO and CO_2 profiles are observed [32]. On the other hand, an increase in oxygenated groups is observed after the PA treatment in all MelPhy samples. In particular, the CO_2 released shows an increase in the contributions associated with the thermal decomposition of CA and LC groups. In addition, it can be assumed that there is some content of basic groups such as Cnyl/QN in the peaks above 900 °C in the CO and CO_2 profiles. In brief, it is observed that the treatment with melamine and phytic acid has effectively incorporated P and N atoms in the RGC-30 carbon, accompanied by a slight oxidation of the carbonaceous material, highlighting the increase of acid groups such as CA and LC, in addition to the generation to a lesser extent of Cnyl/Qn groups.

Table 2
P content of the investigated carbons, as determined by ICP-MS.

Catalyst	P wt.%
MelPhy1.5_900P	5.30
MelPhy2.0_900P	6.08
MelPhy5.0_900P	6.98
RMel_800	N/A
RGC-30	N/A

To better understand the impact of phytic acid and melamine on surface chemistry, we conducted XPS measurements on the investigated carbons. Fig. 5a shows the relative elemental variation of the investigated samples. The introduction of N at the surface level can be observed in the RMel_800 sample, while the surface oxygen content slightly decreases compared to RGC-30. On the other hand, when treating the RMel_800 sample with phytic acid at 900 °C, a decrease in N content is observed, regardless of the amount of phytic acid used. This can be related to the decomposition of nitrogen groups during treatment with PA (temperature used 900 °C) in the form of HCN, as observed during TGA-MS. Furthermore, a bell-shaped trend is observed concerning the surface P content, with the sample MelPhy2.0_900 P exhibiting the highest surface P percentage. This agrees with what was observed during TGA-MS, where the MelPhy2.0_900P sample releases more CO and CO_2 gases associated with P-group decomposition than its counterparts.

XPS spectra in the high-resolution region of C 1s and O 1s show (Fig. S2), as observed by TGA-MS, that RGC-30 is a carbon with a slight degree of oxidation (about 3 at.% surface oxygen). It is composed of a wide variety of C–O, COO, and C=O groups. Upon melamine treatment (RMel_800 sample), the oxygenated groups were still observable in the O 1s region, although the presence of C=O groups was notably reduced compared to the pristine carbon. On the other hand, the N 1s core-level spectrum for the RMel_800 sample (Fig. 5b) shed light on the nitrogen doping of the resulting material. This nitrogen doping primarily consisted of pyridinic-N (398.30 eV) and pyrrolic-N (400.54 eV), with a minor contribution from aminic-N at 399.50 eV, with a total surface N content of 8.13 at. % (Table 4).

The assessment of the C 1s and O 1s regions for MelPhy samples (Fig. S2, Table S1) shows that there is an evolution concerning surface-level oxygenated groups. A stronger signal is observed in the O1s region, indicating an increase in oxygen content. This observation, in line with TGA-MS results, may be associated with slight incorporation of oxygenated groups into the carbon, particularly carboxyls, and lactones, or it could be attributed to various P–O bonds. However, distinguishing whether these oxygenates originate from P- or C-bonded oxygen is challenging due to their closely matching binding energies.

Fig. 5 c depicts the high-resolution XPS spectra of the N 1s and P 2p regions for the co-doped carbons. Within the N 1s core-level (Table 3), we observed contributions from pyridinic-N (about 398.3 ± 0.5 eV) and pyrrolic-N (about 400.4 ± 0.5 eV), accompanied by two notable changes compared to sample RMel_800 [31]. Firstly, there's a reduction in the amount of surface nitrogen groups after treatment, as mentioned above. Secondly, a new contribution emerges at a higher binding energy value, corresponding to a more oxidised N species, quaternary-N (401.7 ± 0.5 eV) [31,33,34]. It is essential to point out that for the MelPhy2.0 and 5.0 samples, there is a small shift to higher binding energies in this new contribution. However, the presence of oxidised N is discarded since, in the O1s region, no corresponding contribution from the oxidised N group could be observed (534.0–534.8 eV) [33]. In addition, in the N-doped and N,P co-doped samples in the C 1s region (Fig. S2 and Table S1), contributions related to C–N bonds of the pyrrolic-N and pyridinic-N groups and C_{sp3}-N related to the quaternary-N are observed in the C 1s region [33,34]. This confirms the presence of these nitrogenous groups in the carbons.

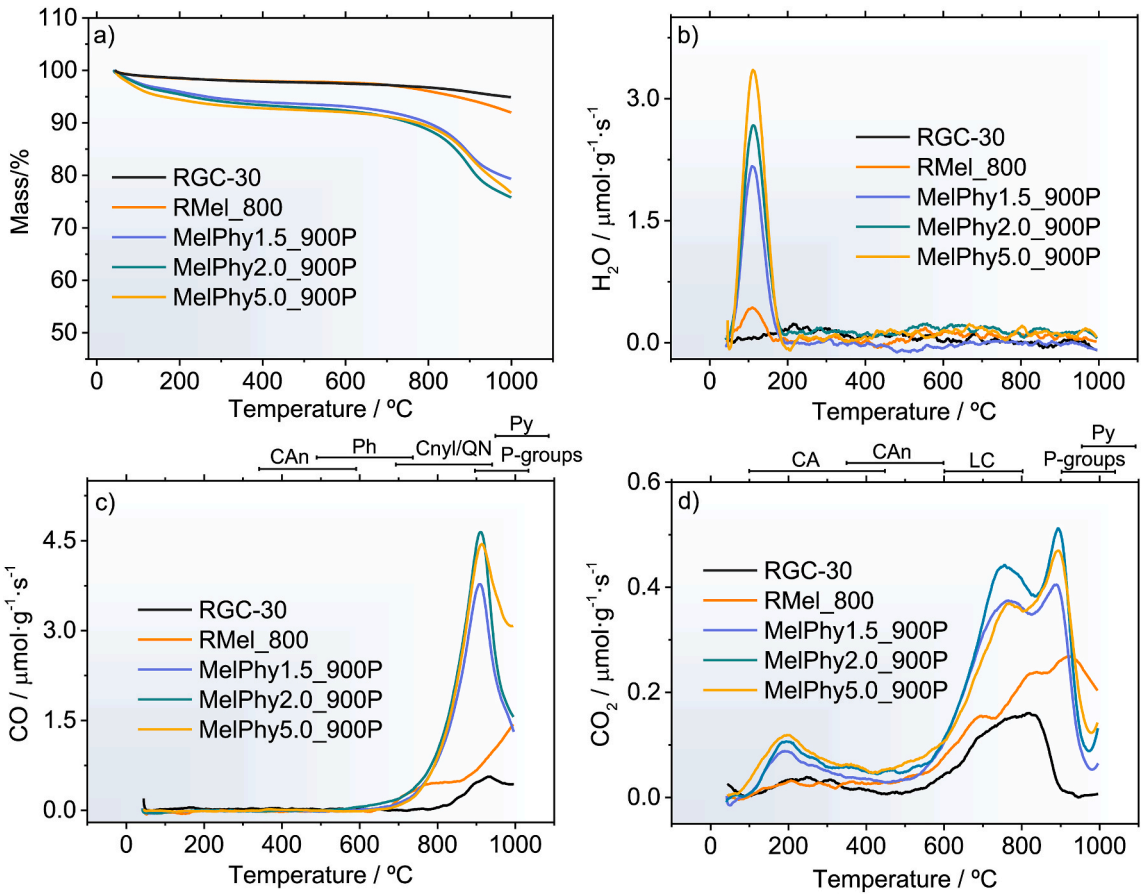

Fig. 4. a) TGA-MS of the N,P doped carbons, RMel_800 and RGC-30 under an inert atmosphere (Ar, 50 ml min^{-1}). Released gases from the studied samples from TGA measurements. b) H_2O (18 m/z), c) CO (28 m/z), d) CO_2 (44 m/z). (A colour version of this figure can be viewed online.)

On the other hand, the deconvolution of the core-level P 2p spectra reveals that all MelPhy carbons exhibit a single surface-level P group (Fig. 5c–Table 4). In the case of samples MelPhy1.5_900P and MelPhy2.0P_900P, this P group can be associated with the C_2PO_2 or CPO_3 species (Table 4) [14,15]. However, distinguishing between these species is challenging due to their overlapping signals at a binding energy of approximately 133.0 eV. In the MelPhy5.0_900P sample, a significantly reduced phosphorus content related to the C_3PO species (132.7 eV) was found [14]. This reduction could indicate that an excess of PA tends to generate a more reduced amount of carbon. Nevertheless, it should be noted that the binding energies of the P atoms in the synthesised materials are remarkably close, suggesting that they have similar electron densities.

The catalysts were tested in the hydrogenation of 1-chloro-4-nitrobenzene (1C–4NB) under mild conditions (80 °C, atmospheric pressure) using hydrazine as a reducing agent (Fig. 6). The blank test shows no catalytic activity from the reactor; however, the RGC-30 carbon shows some catalytic activity, which is associated with its slightly oxidised surface, as observed by TGA-MS and XPS [35]. However, the RMel_800 sample shows an abrupt increase in catalytic activity. As expected, this improvement in activity is due to the nitrogen groups introduced on the surface [36]. However, it should be noted that no consensus has yet been reached on which nitrogen species is the most active. However, an interesting study by Yuqing Chi et al., where they used different treatment ramps to dope carbon nanotubes with chitosan to obtain different N species, found that the most important nitrogen groups in the catalytic activity are pyrrolic-N and quaternary-N [37]. On the other hand, the introduction of P to the catalyst surface shows an improvement in the final conversion, reaching 100 % conversion faster. Finally, as observed in Fig. S3a, all carbons, both doped and undoped, showed a selectivity of 100 % towards the corresponding aniline at all reaction times.

Analysing the correlation between catalytic activity and physicochemical properties, it can be assumed that textural properties do not have a high impact on catalyst performance. The RMel_800 sample exhibits higher catalytic activity than the pristine carbon due to the introduction of N-groups. Conversely, the introduction of P atoms on the catalyst surface (MelPhy samples) enhances the conversion rate of 1-C-4NB. When comparing the surface chemistry of the catalysts, a significant decrease in the N content is observed, together with an increase in the P content, which in turn increases with the amount of PA used during synthesis. However, no clear dependence on phosphorus content and type is observed in the N, P system. As the amount of nitrogen in the MelPhy samples decreases considerably compared to the RMel_800 sample, and the catalytic activity does not decrease, it is presumed that the activity is due to the cooperative effect of the remaining N and P.

Additional catalysts were synthesised to obtain more information on the influence of P on the N–P system, taking the MelPhy1.5_900P sample as a reference. Two catalysts were synthesised at lower temperatures without pre-polymerization (MelPhy1.5_650, MelPhy1.5_800) to obtain different types of surface phosphorus species. In addition, homologous carbons to the MelPhy samples without nitrogen were prepared, following the identical heat treatment with PA applied to MelPhy1.5_900P, MelPhy1.5_800, and MelPhy1.5_650 samples using RGC-30 instead of RMel_800. These resulting samples are denoted as RPhy1.5_900P, RPhy1.5_800, and RPhy1.5_650).

From the catalytic results (Fig. 7), as the MelPhy series, the RPhy carbons showed 100 % selectivity towards 4-chloroaniline (4-CA) (Fig. S3b). Nevertheless, a notable distinction is evident between phosphorous-doped carbons (RPhy samples) and the N, P co-doped ones

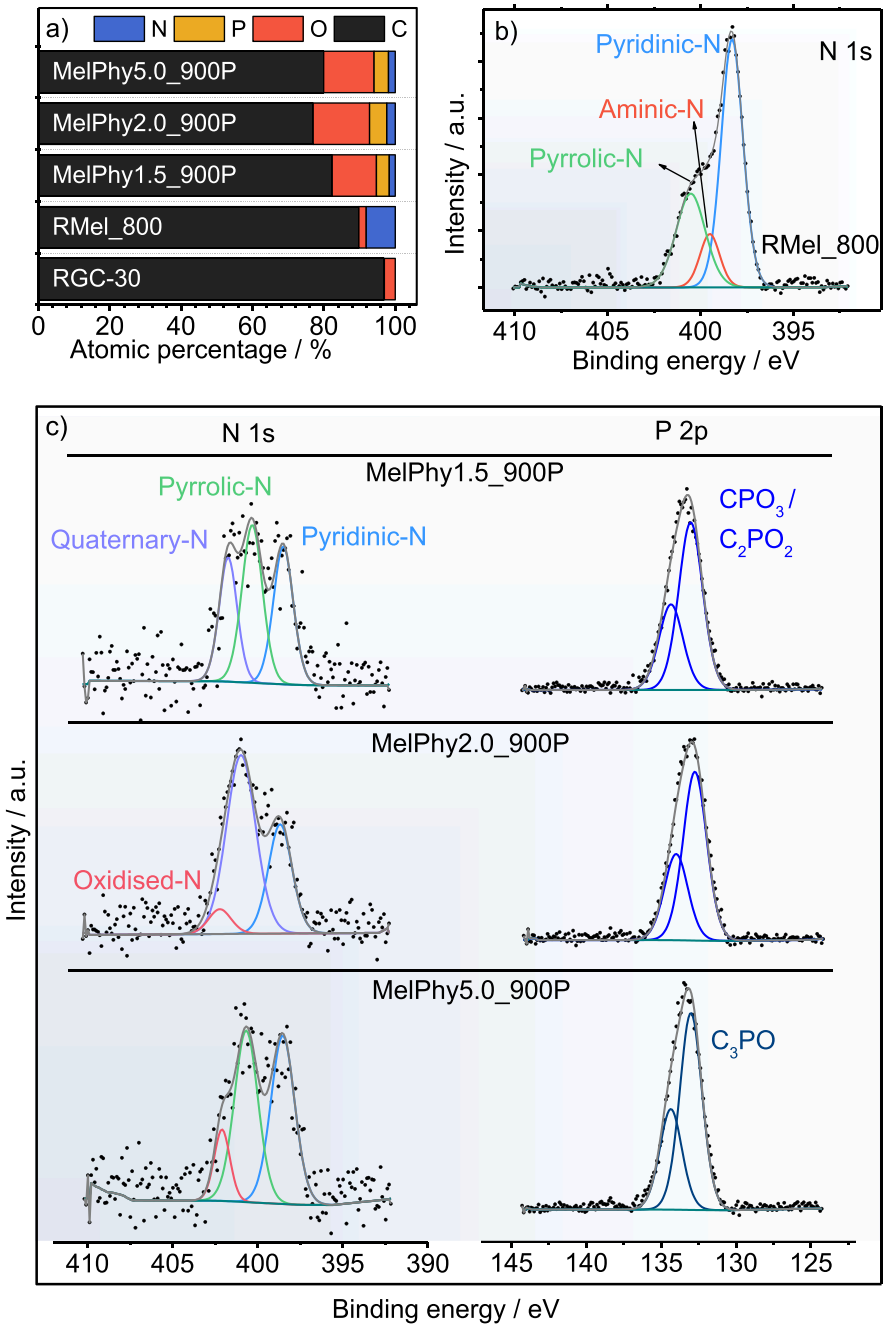

Fig. 5. a) Atomic relative percentage from the XPS data of the investigated carbons. b) N1s core-level for RMel_800 carbon. c) High-resolution XPS spectrum of N, P co-doped carbons with different PA: RMel_800 ratios. (A colour version of this figure can be viewed online.)

(MelPhy samples). All non-nitrogen-containing samples exhibited a lower conversion rate of 1C–4NB. Various characterisation techniques were employed on the new carbons for a more comprehensive understanding of the catalyst's behaviour. The nitrogen adsorption isotherms (Fig. S4) reveal that the catalysts exhibit the same type of isotherm as observed for RGC-30, pointing to a micro-mesoporous carbon. Nevertheless, textural parameters vary depending on the pyrolysis temperature (Table 5). Thus, the most affected parameters by the temperature treatment are microporosity and specific surface area. Three general points can be observed: i) carbons pyrolysed at 650 °C have lower textural properties (this aligns with TGA results showing a more immature carbonisation process than at 800 and 900 °C); ii) porosity recovers with higher treatment temperatures; iii) PA mainly affects micropores. RPhy samples have more developed porosity at 650 and 800 °C due to the higher specific surface area of the starting carbon (RGC-30). However, at 900 °C, both RPhy1.5_900P and MelPhy1.5_900P exhibit similar porosity.

Raman spectroscopy experiments unveiled the presence of D and G bands typical of carbons in all the materials (Figs. S5a and b). XPS measurements (Fig. S6) of the resulting carbons confirm the successful doping and co-doping in both cases. Table 6 Presents the data derived from the deconvoluted high-resolution XPS spectra in the N 1s region. They indicate that the total nitrogen content at 650 and 800 °C stays above 3.5 at.%, decreasing as the temperature rises, with pyrrolic-N being the most prevalent species.

On the other hand, upon analysing the P 2p region (Table 7), it is

Table 3
N 1s core-level resume from N,P co-doped carbons with different PA: RMel_800 ratios.

Catalyst	N-specie	% at. Rel.	Binding energy peak/eV	Total N-content/%
MelPhy1.5_900P	Pyridinic-N	0.56	398.5	1.69
	Pyrrolic-N	0.67	400.3	
	Quaternary-N	0.46	401.7	
MelPhy2.0_900P	Pyridinic-N	0.73	398.7	2.37
	Pyrrolic-N	1.48	400.9	
	Quaternary-N	0.16	402.2	
MelPhy5.0_900P	Pyridinic-N	0.83	398.5	1.90
	Pyrrolic-N	0.84	400.7	
	Quaternary-N	0.23	402.1	
RMel_800	Pyridinic-N	4.77	398.3	8.13
	Aminic-N	0.93	399.5	
	Pyrrolic-N	2.43	400.5	

Table 4
P 2p core-level resume from N, P co-doped carbons with different PA: RMel_800 ratios.

Catalyst	P-specie	% at. Rel.	Binding energy peak/eV
MelPhy1.5_900P	C_2PO_2/CPO_3	3.6	133.0
MelPhy2.0_900P	C_2PO_2/CPO_3	4.82	133.0
MelPhy5.0_900P	C_3PO	4.03	132.7

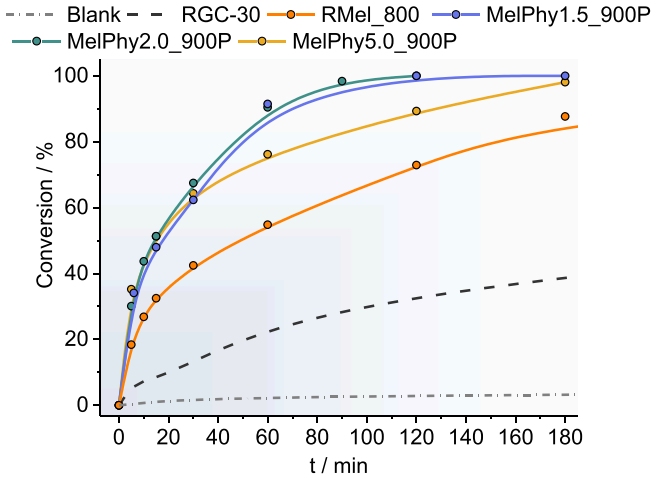

Fig. 6. Catalytic performance of the investigated carbons in the hydrogenation of 1-cloro-4-nitrobenzene. T = 80 °C, 5 mmol of substrate, 100 mg of catalyst, 2 ml of hydrazine. (A colour version of this figure can be viewed online.)

observed, as expected, that different P species could be obtained depending on the treatment. At low temperatures, the main species is $COPO_3$; later, increasing the temperature to 800 °C in the RPhy and MelPhy samples, contributions related to CPO_3/C_2PO_2 emerge [14]. Finally, at high temperatures (900 °C), P is found to be more reduced than in the other cases, in the form of the C_3PO species [14,15]. An important finding is that in samples where the starting carbon already contained nitrogen, a higher surface P content was observed. This may indicate that N promotes the inclusion of P in the carbon to a greater extent. Additionally, in the MelPhy samples, the P species exhibit lower binding energy values compared to the RPhy samples, indicating that P is slightly more reduced in the MelPhy carbons than in the RPhy carbons.

Considering the catalytic results alongside the characterisation

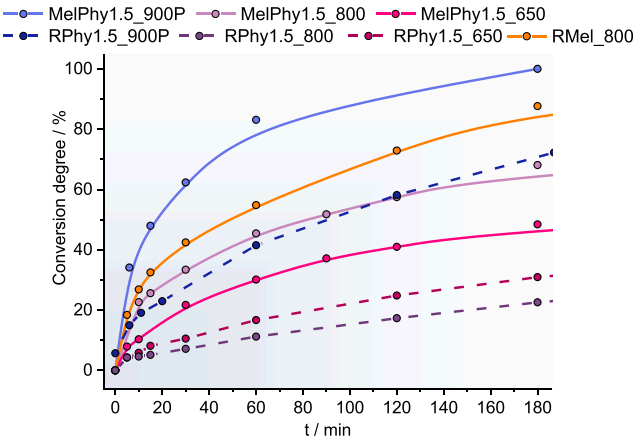

Fig. 7. Catalytic performance comparison of the N, P co-doped, and P-doped carbons in the hydrogenation of 1-cloro-4-nitrobenzene. T = 80 °C, 5 mmol of substrate, 100 mg of catalyst, 2 ml of hydrazine. (A colour version of this figure can be viewed online.)

Table 5
Textural parameters for the N, P- and P- doped samples.

Catalyst	S_{BET} ($m^2 \cdot g^{-1}$)	V_{Total} ($cc \cdot g^{-1}$)	V_{micro} ($cc \cdot g^{-1}$)	V_{meso} ($cc \cdot g^{-1}$)
RPhy1.5_650	242	0.32	0.072	0.25
RPhy1.5_800	957	0.80	0.34	0.46
RPhy1.5_900P	1194	0.91	0.44	0.47
MelPhy1.5_650	115	0.16	0.036	0.12
MelPhy1.5_800	678	0.53	0.23	0.3
MelPhy1.5_900P	1158	0.83	0.39	0.44

Table 6
N 1s core-level resume from N, P co-doped carbons, and P doped carbons.

Catalyst	N-specie	% at. Rel.	Binding energy peak/eV	Total N-content/%
MelPhy1.5_900P	Pyridinic-N	0.56	398.5	1.69
	Pyrrolic-N	0.67	400.3	
	Quaternary-N	0.46	401.7	
MelPhy1.5_850	Pyridinic-N	1.32	398.4	3.66
	Pyrrolic-N	1.58	399.83	
	Quaternary-N	0.76	401.2	
MelPhy1.5_650	Pyridinic-N	0.96	398.4	3.44
	Pyrrolic-N	1.99	400.1	
	Quaternary-N	0.49	401.9	

Table 7
P 2p core-level resume from N, P co-doped carbons, and P doped carbons.

Catalyst	P-specie	% at. Rel.	Binding energy peak/eV
RPhy1.5_650	$COPO_3$	6.92	134.1
RPhy1.5_800	CPO_3/C_2PO_2	1.79	133.7
RPhy1.5_900P	C_3PO	2.82	132.9
MPhy1.5_650	$COPO_3$	8.27	133.9
MelPhy1.5_800	CPO_3/C_2PO_2	4.29	133.1
MelPhy1.5_900P	C_3PO	4.03	132.75

outlined earlier, a clear correlation emerges between the species present and catalytic activity. In all instances, the co-doping of N and P positively impacted substrate conversion. This is noteworthy because, despite the MelPhy samples exhibiting less developed porosity, their catalytic activity surpasses that of the RPhy samples. Furthermore,

MelPhy samples show an activity proportional to the pyrolysis temperature; however, RPhy samples pyrolysed at 800 °C showed lower activity than those treated at 650 °C. However, when normalising the catalytic performance of RPhy catalysts with their P content measured by XPS, the pyrolysis temperature-dependent activity trend is consistent for RPhy and MelPhy catalysts (Fig. S7). Showing that catalysts containing C_3PO are more active. Therefore, the activity organised by the P group can be arranged as follows: C_3PO, C_2PO_2/CPO_3, $COPO_3$. A notable case is observed in the homologous samples RPhy1.5_900P and MelPhy1.5_900P, possessing similar textural properties, but the MelPhy sample clearly performs better than RPhy, showing a significant catalytic difference. Furthermore, despite a lower N content in the MelPhy1.5_900P sample than the RMel_800, the co-doped sample exhibits a higher activity, while in the RPhy1.5_900P sample, the activity is lower. So, a synergistic effect between N and P can be clearly observed. This synergistic effect may be related, on the one hand, to the enhanced adsorption of the nitro group on the N and P groups due to their polarity [16,38]. Furthermore, Xi Jiangbo et al. by DFT study, suggest that the synergistic effect between N and P occurs mainly by altering the charge distribution in the carbonaceous network, given by a negative charge on N atoms and a positive charge on P atoms [9]. In addition, the combined introduction of N and P seems to increase the positive charge of P, which distributes its charge uniformly over the surrounding C atoms [9]. This could be the reason for the synergistic effect, as these C-atoms may play a role as a medium for the transport of protons that react with the nitro group of the substrate.

A recycling test was conducted on the MelPhy samples in the hydrogenation of 1C–4NB, with a reaction time of 15 min, (Fig. 8). After 5 cycles of use, the selectivity towards 4-chloroaniline (4-CA) remained at 100 %. Fig. S8a shows the comparative elemental composition obtained from the sample after five cycles and the fresh sample. Three general changes are observed: the first is a decrease in total P (from 3.6 % to 2.11 %), the second is an increase in surface N (from 1.69 % to 5.57 %), and the third is a decrease in oxygen (from 10.31 % to 12.37 %). These changes indicate that the species most involved during the reaction are P, O and N, with oxygen related to P groups. On the other hand, the increase in surface N is associated with the loss of P, leading to a loss of O, thus leading to an increase in surface N. Otherwise, Fig. S8 b,c shows no variations in species present, such as C3PO and the pyrrole, pyridinic and quaternary N-groups. However, noticeable changes were observed in terms of conversion as the cycles progressed, showing a gradual decrease. This loss in conversion rate may be related to the loss of the active P phase and inherent catalyst mass during each cycle.

4. Conclusions

The prepared nitrogen and phosphorus-doped carbons demonstrated activity in the conversion of 1-chloro-4-nitrobenzene in mono-doped carbons. However, samples with nitrogen and phosphorus surface groups exhibited superior catalytic activity. Regardless of the P functional group, the co-doped carbons outperformed those doped with only P, indicating a synergistic relationship between the two heteroatoms. Nitrogen proved to be crucial, contributing not only to catalytic activity but also resulting in higher final P content in co-doped carbons prepared from N-doped carbons. N,P-doped activated carbons show significant potential as an active, stable, and selective metal-free catalyst in the hydrogenation of 1-chloro-4-nitrobenzene towards 4-chloroaniline.

CRediT authorship contribution statement

Edgar S. Duran-Uribe: Writing – review & editing, Writing – original draft, Methodology, Investigation, Funding acquisition, Formal analysis, Data curation, Conceptualization. **Antonio Sepúlveda-Escribano:** Writing – review & editing, Funding acquisition, Formal analysis, Data curation. **Enrique V. Ramos-Fernandez:** Writing – review & editing, Writing – original draft, Supervision, Formal analysis, Data curation, Conceptualization.

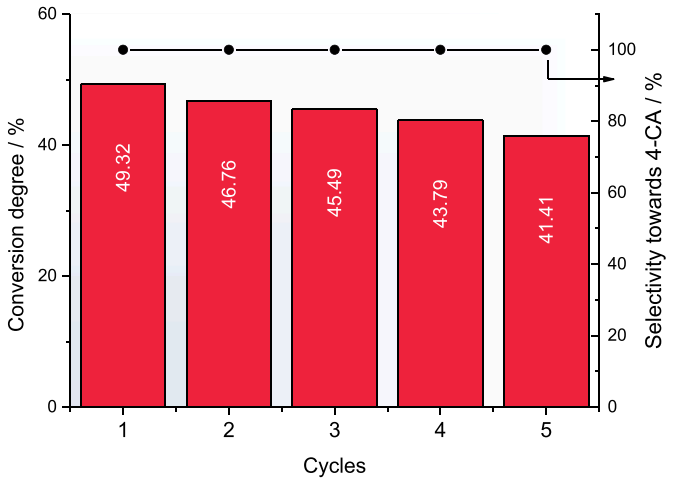

Fig. 8. Recycling test of catalyst MelPhy1.5_900P in the hydrogenation of 1-cloro-nitrobenzene. T = 80 °C, 5 mmol of substrate and 2 ml of hydrazine, at 15 min reaction time. (A colour version of this figure can be viewed online.)

Declaration of competing interest

The authors declare that they have no known competing financial interests or personal relationships that could have appeared to influence the work reported in this paper.

Acknowledgements

The authors gratefully acknowledge the financial support provided by the Ministerio de Ciencia e Innovación (Spain) under Project PID2019-108453 GB-C21 ,PID2020-116998RB-I00. ESDU also thanks the Generalitat Valenciana for their support through grant GRISOLIAP/2020/123. Conselleria de Innovacion, Universidades, Ciencia y Sociedad Digital (CIPROM/2021/022).

Appendix A. Supplementary data

Supplementary data to this article can be found online at https://doi.org/10.1016/j.carbon.2024.119262.

References

[1] R. Gao, C. Peng, J. Zou, Selective catalytic hydrogenation of nitroarenes to anilines, in: Industrial Arene Chemistry, Wiley, 2023, pp. 1479–1524, https://doi.org/10.1002/9783527827992.ch50.
[2] T. Kahl, K.-W. Schröder, F.R. Lawrence, W.J. Marshall, H. Höke, R. Jäckh, Aniline, in: Ullmann's Encyclopedia of Industrial Chemistry, 2000, https://doi.org/10.1002/14356007.a02_303.
[3] J. Song, Z.F. Huang, L. Pan, K. Li, X. Zhang, L. Wang, J.J. Zou, Review on selective hydrogenation of nitroarene by catalytic, photocatalytic and electrocatalytic reactions, Appl. Catal., B 227 (2018) 386–408, https://doi.org/10.1016/j.apcatb.2018.01.052.
[4] J.J. Villora-Picó, I. Campello-Gómez, J.C. Serrano-Ruiz, M.M. Pastor-Blas, A. Sepúlveda-Escribano, E. V Ramos-Fernández, Catalysis Science & Technology Hydrogenation of 4-nitrochlorobenzene catalysed by cobalt nanoparticles supported on nitrogen-doped activated carbon, Catal. Sci. Technol. 11 (2021) 3845, https://doi.org/10.1039/d1cy00140j.
[5] J. Yao, L. Wang, D. Xie, L. Jiang, J. Li, X. Fang, Nanocarbon-based catalysts for selective nitroaromatic hydrogenation: a mini review, Front. Chem. 10 (2022). https://www.frontiersin.org/articles/10.3389/fchem.2022.1000680.
[6] Y. Duan, T. Song, X. Dong, Y. Yang, Enhanced catalytic performance of cobalt nanoparticles coated with a N,P-codoped carbon shell derived from biomass for transfer hydrogenation of functionalised nitroarenes, Green Chem. 20 (2018) 2821–2828, https://doi.org/10.1039/C8GC00619A.
[7] Y. Rangraz, M.M. Heravi, Recent advances in metal-free heteroatom-doped carbon heterogonous catalysts, RSC Adv. 11 (2021) 23725–23778, https://doi.org/10.1039/D1RA03446D.

[8] T.J. Bandosz, C.O. Ania, Chapter 4 Surface chemistry of activated carbons and its characterisation, in: T.J. Bandosz (Ed.), Interface Science and Technology, Elsevier, 2006, pp. 159–229, https://doi.org/10.1016/S1573-4285(06)80013-X.
[9] J. Xi, Q. Wang, J. Liu, L. Huan, Z. He, Y. Qiu, J. Zhang, C. Tang, J. Xiao, S. Wang, N, P-dual-doped multilayer graphene as an efficient carbocatalyst for nitroarene reduction: a mechanistic study of metal-free catalysis, J. Catal. 359 (2018) 233–241, https://doi.org/10.1016/j.jcat.2018.01.003.
[10] J.P. Paraknowitsch, A. Thomas, Doping carbons beyond nitrogen: an overview of advanced heteroatom doped carbons with boron, sulphur and phosphorus for energy applications, Energy Environ. Sci. 6 (2013) 2839–2855, https://doi.org/10.1039/C3EE41444B.
[11] Y. Yang, L. Gu, S. Guo, S. Shao, Z. Li, Y. Sun, S. Hao, N-doped mesoporous carbons: from synthesis to applications as metal-free reduction catalysts and energy storage materials, Front. Chem. 7 (2019). https://www.frontiersin.org/articles/10.3389/fchem.2019.00761.
[12] E. Lepre, S. Rat, C. Cavedon, P.H. Seeberger, B. Pieber, M. Antonietti, N. López-Salas, Catalytic properties of high nitrogen content carbonaceous materials, Angew. Chem. Int. Ed. 62 (2023) e202211663, https://doi.org/10.1002/anie.202211663.
[13] J. Shan, X. Sun, S. Zheng, T. Wang, X. Zhang, G. Li, Graphitic N-dominated nitrogen-doped carbon nanotubes as efficient metal-free catalysts for hydrogenation of nitroarenes, Carbon N Y 146 (2019) 60–69, https://doi.org/10.1016/j.carbon.2019.01.103.
[14] A.M. Puziy, O.I. Poddubnaya, B. Gawdzik, J.M.D. Tascón, Phosphorus-containing carbons: preparation, properties and utilisation, Carbon N Y 157 (2020) 796–846, https://doi.org/10.1016/j.carbon.2019.10.018.
[15] Y. Li, H. Zhao, S. Chen, S. Bao, F. Xing, B. Jiang, Phosphorus-doped activated carbon catalyst for n-hexane dehydroaromatization reaction, Catal. Commun. 156 (2021) 106318, https://doi.org/10.1016/j.catcom.2021.106318.
[16] R. Gao, L. Pan, J. Lu, J. Xu, X. Zhang, L. Wang, J.-J. Zou, Phosphorus-doped and lattice-defective carbon as metal-like catalyst for the selective hydrogenation of nitroarenes, ChemCatChem 9 (2017) 4287–4294, https://doi.org/10.1002/cctc.201700904.
[17] X. Chen, Q. Shen, Z. Li, W. Wan, J. Chen, J. Zhang, Metal-free H2 activation for highly selective hydrogenation of nitroaromatics using phosphorus-doped carbon nanotubes, ACS Appl. Mater. Interfaces 12 (2020) 654–666, https://doi.org/10.1021/acsami.9b17582.
[18] S. Liu, L. Cui, Z. Peng, J. Wang, Y. Hu, A. Yu, H. Wang, P. Peng, F.-F. Li, Eco-friendly synthesis of N,S co-doped hierarchical nanocarbon as a highly efficient metal-free catalyst for the reduction of nitroarenes, Nanoscale 10 (2018) 21764–21771, https://doi.org/10.1039/C8NR07083K.
[19] H. Zhang, C. Zhang, Y. Zhang, P. Cui, Y. Zhang, L. Wang, H. Wang, Y. Gao, P/N co-doped carbon derived from cellulose: a metal-free photothermal catalyst for transfer hydrogenation of nitroarenes, Appl. Surf. Sci. 487 (2019) 616–624, https://doi.org/10.1016/j.apsusc.2019.05.144.
[20] F. Hassanzadeh-Afruzi, H. Dogari, F. Esmailzadeh, A. Maleki, Magnetized melamine-modified polyacrylonitrile (PAN@melamine/Fe3O4) organometallic nanomaterial: preparation, characterization, and application as a multifunctional catalyst in the synthesis of bioactive dihydropyrano [2,3-c]pyrazole and 2-amino-3-cyano 4H-pyran derivatives, Appl. Organomet. Chem. 35 (2021) e6363, https://doi.org/10.1002/aoc.6363.
[21] H. Yan, Y. Chen, S. Xu, Synthesis of graphitic carbon nitride by directly heating sulfuric acid treated melamine for enhanced photocatalytic H2 production from water under visible light, Int. J. Hydrogen Energy 37 (2012) 125–133, https://doi.org/10.1016/j.ijhydene.2011.09.072.
[22] Y.C. Zhao, D.L. Yu, H.W. Zhou, Y.J. Tian, O. Yanagisawa, Turbostratic carbon nitride prepared by pyrolysis of melamine, J. Mater. Sci. 40 (2005) 2645–2647, https://doi.org/10.1007/s10853-005-2096-3.
[23] A.L.M. Daneluti, J. do R. Matos, Study of thermal behavior of phytic acid, Brazilian Journal of Pharmaceutical Sciences 49 (2013).
[24] M. Thommes, K. Kaneko, A. V Neimark, J.P. Olivier, F. Rodriguez-Reinoso, J. Rouquerol, K.S.W. Sing, Physisorption of gases, with special reference to the evaluation of surface area and pore size distribution, IUPAC Technical Report) 87 (2015) 1051–1069, https://doi.org/10.1515/pac-2014-1117.
[25] W. Luo, B. Wang, C.G. Heron, M.J. Allen, J. Morre, C.S. Maier, W.F. Stickle, X. Ji, Pyrolysis of cellulose under ammonia leads to nitrogen-doped nanoporous carbon generated through methane formation, Nano Lett. 14 (2014) 2225–2229, https://doi.org/10.1021/nl500859p.
[26] A.C. Ferrari, J. Robertson, Interpretation of Raman spectra of disordered and amorphous carbon, Phys. Rev. B 61 (2000) 14095–14107, https://doi.org/10.1103/PhysRevB.61.14095.
[27] A. Sadezky, H. Muckenhuber, H. Grothe, R. Niessner, U. Pöschl, Raman microspectroscopy of soot and related carbonaceous materials: spectral analysis and structural information, Carbon N Y 43 (2005) 1731–1742, https://doi.org/10.1016/j.carbon.2005.02.018.
[28] O. Beyssac, B. Goffé, J.-P. Petitet, E. Froigneux, M. Moreau, J.-N. Rouzaud, On the characterization of disordered and heterogeneous carbonaceous materials by Raman spectroscopy, Spectrochim. Acta Mol. Biomol. Spectrosc. 59 (2003) 2267–2276, https://doi.org/10.1016/S1386-1425(03)00070-2.
[29] G. Daniel, T. Kosmala, M.C. Dalconi, L. Nodari, D. Badocco, P. Pastore, A. Lorenzetti, G. Granozzi, C. Durante, Upcycling of polyurethane into iron-nitrogen-carbon electrocatalysts active for oxygen reduction reaction, Electrochim. Acta 362 (2020) 137200, https://doi.org/10.1016/j.electacta.2020.137200.
[30] H. Marsh, F. Rodríguez-Reinoso, Activated carbon (origins), in: H. Marsh, F. Rodríguez-Reinoso (Eds.), Activated Carbon, Elsevier, Oxford, 2006, pp. 13–86, https://doi.org/10.1016/B978-008044463-5/50016-9.
[31] R.P. Rocha, M.F.R. Pereira, J.L. Figueiredo, Characterisation of the surface chemistry of carbon materials by temperature-programmed desorption: an assessment, Catal. Today 418 (2023) 114136, https://doi.org/10.1016/j.cattod.2023.114136.
[32] N. Rey-Raap, M.A.C. Granja, M.F.R. Pereira, J.L. Figueiredo, Phosphorus-doped carbon/carbon nanotube hybrids as high-performance electrodes for supercapacitors, Electrochim. Acta 354 (2020) 136713, https://doi.org/10.1016/j.electacta.2020.136713.
[33] T. Kato, Y. Yamada, Y. Nishikawa, T. Otomo, H. Sato, S. Sato, Origins of peaks of graphitic and pyrrolic nitrogen in N1s X-ray photoelectron spectra of carbon materials: quaternary nitrogen, tertiary amine, or secondary amine? J. Mater. Sci. 56 (2021) 15798–15811, https://doi.org/10.1007/s10853-021-06283-5.
[34] M. Ayiania, M. Smith, A.J.R. Hensley, L. Scudiero, J.-S. McEwen, M. Garcia-Perez, Deconvoluting the XPS spectra for nitrogen-doped chars: an analysis from first principles, Carbon N Y 162 (2020) 528–544, https://doi.org/10.1016/j.carbon.2020.02.065.
[35] J.C. Espinosa, S. Navalon, M. Alvaro, A. Dhakshinamoorthy, H. Garcia, Reduction of C═C double bonds by hydrazine using active carbons as metal-free catalysts, ACS Sustain. Chem. Eng. 6 (2018) 5607–5614, https://doi.org/10.1021/acssuschemeng.8b00638.
[36] W. Xiong, Z. Wang, S. He, F. Hao, Y. Yang, Y. Lv, W. Zhang, P. Liu, H. Luo, Nitrogen-doped carbon nanotubes as a highly active metal-free catalyst for nitrobenzene hydrogenation, Appl. Catal., B 260 (2020) 118105, https://doi.org/10.1016/j.apcatb.2019.118105.
[37] Y. Chi, S. Zheng, X. Zhang, G. Li, Chitosan derived N-doped carbon nanotubes for selective hydrogenation of nitroarenes to anilines, Int. J. Hydrogen Energy 46 (2021) 36124–36136, https://doi.org/10.1016/j.ijhydene.2021.08.136.
[38] M. Tamura, K. Shimizu, A. Satsuma, Comprehensive IR study on acid/base properties of metal oxides, Appl. Catal. Gen. 433–434 (2012) 135–145, https://doi.org/10.1016/j.apcata.2012.05.008.